Light clusters in nuclear matter and the "pasta" phase

S. S. Avancini,[1] C. C. Barros Jr.,[1] L. Brito,[2] S. Chiacchiera,[2] D. P. Menezes,[1] and C. Providência[2]
[1]*Departamento de Física, CFM, Universidade Federal de Santa Catarina Florianópolis, SC, Caixa Postal 476, CEP 88.040-900, Brazil*
[2]*Centro de Física Computacional, Department of Physics, University of Coimbra, P-3004-516 Coimbra, Portugal*
(Received 18 November 2011; revised manuscript received 9 January 2012; published 23 March 2012)

The effects of including light clusters in nuclear matter at low densities are investigated within four different parametrizations of relativistic models at finite temperature. Both homogeneous and inhomogeneous matter (pasta phase) are described for neutral nuclear matter with fixed proton fractions. We discuss the effect of the density dependence of the symmetry energy, the temperature, and the proton fraction on the nonhomogeneous matter forming the inner crust of protoneutron stars. It is shown that the number of nucleons in the clusters, the cluster proton fraction, and the sizes of the Wigner-Seitz cell and of the cluster are very sensitive to the density dependence of the symmetry energy.

DOI: 10.1103/PhysRevC.85.035806 PACS number(s): 21.65.−f, 24.10.Jv, 26.60.−c, 95.30.Tg

I. INTRODUCTION

The formation of light clusters in nuclear matter at low densities and its influence on the appearance and composition of pasta structures has been frequently discussed in the literature [1–10].

Below saturation density, homogeneous nuclear matter can become unstable against phase separation and several types of complex structures can be formed as a result of the competition between the strong and the electromagnetic interactions. This "pasta" phase [11–15] is found at densities of the order of 0.001–0.1 fm^{-3} [16] in neutral nuclear matter, formed by protons, neutrons, and electrons, and in a smaller density range in β-equilibrium stellar matter [17,18]. At very low densities, up to 0.001 times the saturation density, and moderate temperatures, the few-body correlations are still important and the system minimizes its energy by forming light nuclei such as deuterons, tritons, helions, and/or α particles. The appearance of these light clusters can modify the behavior of the neutrinos in the expanding matter resulting from a supernovae core collapse and affect the cooling process of the protoneutron star.

In a previous paper [19] we have studied the influence of the α particles both on homogeneous matter and on the onset and structure of the pasta phase within the relativistic mean-field approximation. We have considered both free α particles and α particles interacting through an α-ω meson coupling. This repulsive interaction is essential to avoid an overprediction of α particles above $\rho \sim 0.001$ fm^{-3} and it is also the mechanism responsible for the dissolution of the α-particle clusters in the approach considered.

Model dependencies are more important for $\rho > 0.001$ fm^{-3} when the α-particle fraction differences between models may be as large as one order of magnitude or even larger. The effect of the temperature is to shift the maximum of the α-particle distribution and the density of cluster dissolution to larger densities. At the same time, the maximum values of the distributions themselves were shown to decrease with the increase of the temperature. The maximum values of the α-particle distributions also decrease when the proton fraction decreases. However, the proton fraction has no effect either on the density localization of the maximum or on the density of dissolution of the clusters.

It was also shown that in the pasta phase formed in asymmetric nuclear matter the α-particle fraction increases with temperature. This is an interesting effect related to the proton fraction in the background gas, which increases with temperature for asymmetric matter. It is important to test the above-mentioned behaviors when other light clusters are also included in the system.

In the present paper we extend our previous work [19] by considering also deuterons, tritons, and helions. We study the distribution of these light clusters as a function of the baryonic density for several temperatures and proton fractions, and we investigate the effect of the light clusters on the onset, type of structures, and size of the heavy clusters ($A > 4$) of the pasta phase. We compute the mass and charge content of the droplets formed in the droplet regime of the pasta phase and compare with other approaches.

Our approach to the description of the pasta phase is within what is known as the single-nucleus approximation. The same approach was used in [1,2]; however, only α particles were included as light clusters. In [7] a statistical model consisting of an ensemble of nuclei and interacting nucleons in nuclear statistical equilibrium was proposed to describe supernova matter. There, it was shown that the presence of light clusters besides α particles is of particular importance at low densities. A similar conclusion was drawn in [8], where a phenomenological statistical model consisting of free nucleons described within a mean-field approximation and a loosely interacting cluster gas was formulated to describe matter in supernova explosions and protoneutron stars. In all these works an excluding volume concept was used: in the first two works this was done with respect to the α particles and in the other two with respect to all nuclei or clusters.

The validity of the two approximations, excluded volume and single nucleus, has already been discussed. Recently, the excluded volume approach was compared to two quantum many-body models in [10] and it was shown that this approach is a bit crude at temperatures of the order of 5 MeV, although this occurs at densities where the composition of

matter is dominated by heavy ions. In [20] it was discussed that the equation of state (EOS) is not much affected by the single-nucleus approximation, which describes matter composition in an average way, although a correct distribution of nuclei may be important to describe correctly the supernova dynamics.

The approach we consider in the present work has the drawbacks of a single-nucleus approximation and does not include shell effects, in contrast to statistical models [10]. Therefore, we will restrict ourselves to temperatures above which shell effects are no longer important. However, we would like to point out that at densities close to the crust-core transition statistical models have difficulties in describing properly the medium effects on the nuclei and exotic structures such as the pasta phases, in contrast to the present approach.

As mentioned before, we will avoid the excluded volume approximation and will include Pauli blocking and self-energy effects in a phenomenological approach by including a meson-cluster interaction within a relativistic mean-field formalism. A quantum statistical approach allows the calculation of the medium influence on the quasienergies of clusters [3,6,9]. In particular, recently, analytical fits to the quasienergy shifts of light nuclei were published [9]. These results allow the determination of a better parametrization of the cluster-meson interaction than the one used in the present work. However, we should point out that when the medium effects are more important the contribution of light clusters is already very small. Moreover, we have shown in [19] that the fraction of α particles obtained with the prescription used in the present work agrees with the results both of the virial equation proposed in [4] and the results of [6] within a generalized mean-field model.

A relativistic mean-field approach is a phenomenological theory where the meson-nucleon and the meson-meson interactions mimic the different contributions of a quantum many-body formalism such as the Pauli blocking and self-energies and it is difficult to separate the different contributions which determine the behavior of the system. The same may be said with respect to the meson-cluster interactions introduced in [6,19]. In a recent study [21] the effect of the meson-cluster couplings in the EOS of homogeneous nuclear matter with clusters was investigated within a zero-temperature relativistic mean-field approach. It was shown that the σ-cluster and ω-cluster couplings determine the behavior of the clusters, namely their fraction and dissolution density.

In this work we use the relativistic mean-field approximation and we consider four different parametrizations. We have chosen the NL3 [22], NL3$\omega\rho$ [23], FSU$_{\rm Gold}$ [24], and IU-FSU [25] parametrizations of the nonlinear Walecka model (NLWM) [26], which allow us to discuss the role of the density dependence of the symmetry energy on the properties of the nonhomogeneous nuclear EOS.

The paper is organized as follows: in Sec. II we briefly review the formalism underlying the homogeneous neutral *npe* matter with the inclusion of the light clusters. In Sec. III the coexisting-phases method used to obtain the pasta phase is briefly reviewed. In Sec. IV our results are displayed and commented upon and in Sec. V the final conclusions are drawn.

II. FORMALISM

We consider a system of protons and neutrons with mass M interacting with and through an isoscalar-scalar field ϕ with mass m_s, an isoscalar-vector field V^μ with mass m_v, and an isovector-vector field $\mathbf{b}^\mu$ with mass m_ρ. We also include tritons (^{3}H, represented by t), helions (^{3}He, represented by h), α particles, and deuterons (d). A system of electrons with mass m_e that makes matter neutral is also included.

The Lagrangian density reads

$$\mathcal{L} = \sum_{j=p,n,t,h} \mathcal{L}_j + \mathcal{L}_\alpha + \mathcal{L}_d + \mathcal{L}_\sigma + \mathcal{L}_\omega + \mathcal{L}_\rho + \mathcal{L}_{\omega\rho} + \mathcal{L}_e + \mathcal{L}_A, \tag{1}$$

where the Lagrangian density $\mathcal{L}_j$ is

$$\mathcal{L}_j = \bar{\psi}_j\left[\gamma_\mu i D_j^\mu - M_j^*\right]\psi_j. \tag{2}$$

The α particles and the deuterons are described as in [6] with $\mathcal{L}_\alpha$ and $\mathcal{L}_d$ given, respectively, by

$$\mathcal{L}_\alpha = \tfrac{1}{2}\left(i D_\alpha^\mu \phi_\alpha\right)^*\left(i D_{\mu\alpha}\phi_\alpha\right) - \tfrac{1}{2}\phi_\alpha^* M_\alpha^2 \phi_\alpha \tag{3}$$

and

$$\mathcal{L}_d = \tfrac{1}{4}\left(i D_d^\mu \phi_d^\nu - i D_d^\nu \phi_d^\mu\right)^*\left(i D_{d\mu}\phi_{d\nu} - i D_{d\nu}\phi_{d\mu}\right) - \tfrac{1}{2}\phi_d^{\mu *} M_d^2 \phi_{d\mu}, \tag{4}$$

with

$$i D_j^\mu = i\partial^\mu - g_{vj} V^\mu - \frac{g_{\rho j}}{2}\boldsymbol{\tau}\cdot\mathbf{b}^\mu - \frac{e}{2}(1+\tau_3)A^\mu, \quad j = p, n, t, h, \alpha, d, \tag{5}$$

$$M_j^* = M - g_s\phi, \quad j = p, n, \tag{6}$$

$$M_t^* = M_t = 3M - B_t, \tag{7}$$

$$M_h^* = M_h = 3M - B_h, \tag{8}$$

$$M_\alpha^* = M_\alpha = 4M - B_\alpha, \tag{9}$$

$$M_d^* = M_d = 2M - B_d, \tag{10}$$

with the binding energies given by $B_t = 8.482$ MeV, $B_h = 7.718$ MeV, $B_\alpha = 28.296$ MeV, and $B_d = 2.224$ MeV and $g_{vj} = A_j g_v$ and $g_{\rho j} = |Z_j - N_j| g_\rho$, where A_j is the mass number, Z_j is the proton number, and N_j is the neutron number. Notice that in our model the cluster masses are fixed to constant values: they do not depend upon the temperature and the density. However, due to the cluster-meson interaction, we find (see Sec. IV) that the dissolution density of each cluster increases with the temperature.

The electron Lagrangian density is given by

$$\mathcal{L}_e = \bar{\psi}_e[\gamma_\mu(i\partial^\mu + eA^\mu) - m_e]\psi_e, \tag{11}$$

and the remaining terms in Eq. (1) are

$$\mathcal{L}_\sigma = +\tfrac{1}{2}\left(\partial_\mu\phi\partial^\mu\phi - m_s^2\phi^2 - \tfrac{1}{3}\kappa\phi^3 - \tfrac{1}{12}\lambda\phi^4\right),$$
$$\mathcal{L}_\omega = \tfrac{1}{2}\left(-\tfrac{1}{2}\Omega_{\mu\nu}\Omega^{\mu\nu} + m_v^2 V_\mu V^\mu + \tfrac{1}{12}\xi g_v^4 (V_\mu V^\mu)^2\right),$$
$$\mathcal{L}_\rho = \tfrac{1}{2}\left(-\tfrac{1}{2}\mathbf{B}_{\mu\nu}\cdot\mathbf{B}^{\mu\nu} + m_\rho^2 \mathbf{b}_\mu\cdot\mathbf{b}^\mu\right),$$

$$\mathcal{L}_{\omega\rho} = \Lambda_v g_v^2 g_\rho^2 V_\mu V^\mu \mathbf{b}_\mu \cdot \mathbf{b}^\mu,$$
$$\mathcal{L}_A = -\tfrac{1}{4} F_{\mu\nu} F^{\mu\nu},$$

where $\Omega_{\mu\nu} = \partial_\mu V_\nu - \partial_\nu V_\mu$, $\mathbf{B}_{\mu\nu} = \partial_\mu \mathbf{b}_\nu - \partial_\nu \mathbf{b}_\mu - \Gamma_\rho(\mathbf{b}_\mu \times \mathbf{b}_\nu)$, and $F_{\mu\nu} = \partial_\mu A_\nu - \partial_\nu A_\mu$. The parameters of the models are the nucleon mass $M = 939$ MeV, the coupling parameters g_s, g_v, and g_ρ of the mesons to the nucleons, the self interacting κ, λ, and ξ constant couplings, and the ω-ρ coupling Λ_v. In the above Lagrangian density $\boldsymbol{\tau}$ is the isospin operator. When the NL3 parametrization is used, Λ_v is set equal to zero. When the NL3$\omega\rho$ parametrization is chosen, we follow the prescription of [23], where the starting point was the NL3 parametrization and the g_ρ coupling was adjusted for each value of the coupling Λ_v in such a way that for $k_F = 1.15\ \mathrm{fm}^{-1}$ (not the saturation point) the symmetry energy is 25.68 MeV. In particular, in this work we set Λ_v to a moderately large value ($\Lambda_v = 0.03$; see Table I). The comparison of NL3 and NL3$\omega\rho$ results is meant to show the effect of changing the isovector part of the Lagrangian only.

The $\mathrm{FSU_{Gold}}$ [24] parametrization was chosen because it has the advantage of reproducing some of the results [27] obtained with more sophisticated density dependent hadronic models [28] without the need of rearrangement terms. $\mathrm{FSU_{Gold}}$ combines the inclusion of the vector self-interaction term present in Refs. [29,30] that is responsible for explaining some observed properties at nuclear density and the isoscalar-isovector coupling present in [23], capable of improving the density dependence of the symmetry energy. An interesting comparison of the results for the neutron star mass-radius relation involving NL3 and $\mathrm{FSU_{Gold}}$ is given in [31]. We also consider the IU-FSU parametrization, which keeps the main properties of FSU but was readjusted in order to allow for neutron star masses up to about $2.0 M_\odot$ [25]. The parameter sets for the NL3, NL3$\omega\rho$, $\mathrm{FSU_{Gold}}$, and IU-FSU models are shown in Table I. Their corresponding bulk nuclear matter properties are given in Table II. In order to clarify the discussion, we show in Fig. 1, for the models considered, the symmetry energy at densities below $0.3\ \mathrm{fm}^{-3}$ and the surface tension at $T = 5$ MeV as a function of the proton fraction. The surface tension was determined according to the parametrization given in Eq. (33)

TABLE I. Parameter sets for the models used in this work. The masses of the mesons are in MeV and the other quantities are dimensional (with κ given in nucleon mass units).

	NL3 [22]	NL3$\omega\rho$ [23]	$\mathrm{FSU_{Gold}}$ [24]	IU-FSU [25]
m_s	508.194	508.194	491.500	491.500
m_v	782.501	782.501	782.500	782.500
m_ρ	763.000	763.000	763.000	763.000
g_s	10.217	10.217	10.592	9.971
g_v	12.868	12.868	14.302	13.032
g_ρ	8.948	11.2766	11.767	13.590
κ	4.384	4.384	1.7976	3.5695
λ	−173.31	−173.31	299.11	2.926
ξ	0.00	0.00	0.06	0.03
Λ_v	0.00	0.03	0.03	0.046

TABLE II. Nuclear matter properties at the saturation density and zero temperature: binding energy per nucleon, B/A, density ρ_0, effective nucleon mass M^*, incompressibility K, symmetry energy $\mathcal{E}_{\mathrm{sym}}$, and slope L of the symmetry energy $\mathcal{E}_{\mathrm{sym}}(\rho)$.

	NL3 [22]	NL3$\omega\rho$ [23]	$\mathrm{FSU_{Gold}}$ [24]	IU-FSU [25]
B/A (MeV)	16.3	16.3	16.302	16.4
ρ_0 (fm^{-3})	0.148	0.148	0.148	0.155
M^*/M	0.60	0.60	0.62	0.62
K (MeV)	272	272	227.9	231.2
$\mathcal{E}_{\mathrm{sym}}$ (MeV)	37.4	31.66	32.54	31.3
L (MeV)	118.32	55.23	60.39	47.2

and the Appendix. With the present choice of models we will be able to discuss the implications of the symmetry energy on the pasta phase. One expects, generally speaking, two types of effects: a smaller L corresponds to a larger surface tension for asymmetric matter [see Fig. 1(b) and Table II]; a larger $\mathcal{E}_{\mathrm{sym}}$ leads to a more isospin-symmetric liquid phase. We will see in Sec. IV that in models with a larger surface tension the pasta phase sets in at higher densities and the drip of particles is unfavored, giving rise to a lower density background gas.

After this discussion that motivates our choice of parametrizations, we go back to the description of the method. From the Euler-Lagrange formalism we obtain coupled differential equations for the scalar, vector, isovector-scalar, nucleon, and cluster fields. In the static case there are no currents and the spatial vector components are zero. Moreover, we neglect, as usual, the Coulomb interaction in the case of homogeneous matter. In the calculation of the pasta phase, its effect on the protons will be included. In [16] a complete description of the mean-field and Thomas-Fermi approximations applied to different parametrizations of the NLWM is given and we do not repeat it here. The equations of motion for the fields are obtained and solved self-consistently and they can be read off [16,18]. The above-mentioned equations of motion depend on the the equilibrium densities

$$\rho = \rho_p + \rho_n + 4\rho_\alpha + 2\rho_d + 3\rho_t + 3\rho_h, \quad (12)$$
$$\rho_3 = \rho_p - \rho_n - \rho_t + \rho_h, \quad (13)$$
$$\rho_s = \rho_{s_p} + \rho_{s_n}. \quad (14)$$

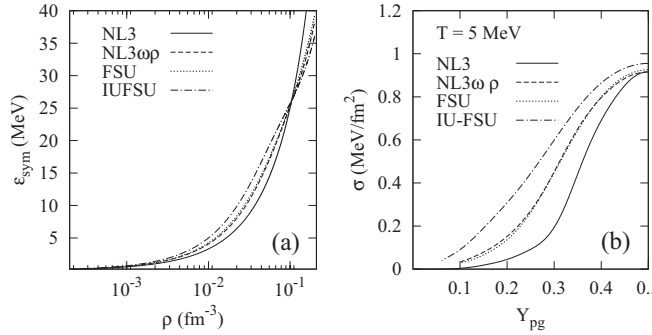

FIG. 1. Comparison of (a) the symmetry energy and (b) the surface tension at $T = 5$ MeV calculated with the models NL3, NL3$\omega\rho$, $\mathrm{FSU_{Gold}}$, and IU-FSU.

The quantities ρ_α and ρ_d are discussed next. The fermionic densities are

$$\rho_i = \frac{1}{\pi^2}\int p^2 dp (f_{i+} - f_{i-}),\ \ i = p, n, t, h, \tag{15}$$

and the corresponding scalar densities are

$$\rho_{s_i} = \frac{1}{\pi^2}\int p^2 dp \frac{M_i^*}{\epsilon_i^*}(f_{i+} + f_{i-}). \tag{16}$$

The distribution functions are given by

$$f_{i\pm} = \frac{1}{1 + \exp[(\epsilon_i^*(\mathbf{p}) \mp \nu_i)/T]}\ , \quad i = p, n, t, h, \tag{17}$$

where $\epsilon_i^* = \sqrt{\mathbf{p}^2 + M_i^{*2}}$, and the effective chemical potentials are

$$\nu_i = \mu_i - g_{vi} V_0 - \frac{g_{\rho i}}{2}\tau_{3i} b_0, \tag{18}$$

where

$$\mu_t = \mu_p + 2\mu_n, \quad \mu_h = 2\mu_p + \mu_n, \tag{19}$$

and $\tau_{3i} = \pm 1$ is the isospin projection for the protons (helions) and neutrons (tritons), respectively.

In the present work the α particles and the deuterons are included as bosons and their chemical potentials are obtained from the proton and neutron chemical potentials by imposing chemical equilibrium, as in [6]:

$$\mu_\alpha = 2(\mu_p + \mu_n), \quad \mu_d = \mu_p + \mu_n. \tag{20}$$

Their effective chemical potentials read

$$\nu_j = \mu_j - g_j V_0, \quad j = \alpha, d. \tag{21}$$

The density of thermal α particles and deuterons is

$$\rho_j = \frac{1}{\pi^2}\int p^2 dp (f_{j+} - f_{j-}), \tag{22}$$

with the boson distribution function given by

$$f_{j\pm} = \frac{1}{-1 + \exp[(\epsilon_j \mp \nu_j)/T]}, \tag{23}$$

where $\epsilon_j = \sqrt{p^2 + M_j^2}$. We should point out that at low enough temperatures the α particles and deuterons contribute with two terms: a condensed fraction and a thermal contribution. Both contributions can be included explicitly in the present formalism. We only indicate the thermal contribution because we have limited our discussion to temperatures above Bose condensation of α particles or deuterons.

For the free electrons, their density and distribution functions are the same as for the other fermions, where μ_e is the electron chemical potential and $\epsilon_e = \sqrt{p^2 + m_e^2}$. We always consider neutral matter and therefore the electron density is equal to the total charge density of the charged particles.

In the description of the equation of state of a system, the required quantities are the baryonic density ρ, energy density $\mathcal{E}$, entropy density $\mathcal{S}$, pressure P, and free energy density $\mathcal{F} = \mathcal{E} - T\mathcal{S}$, and their expressions are explicitly given in [16,18].

III. NUCLEAR PASTA

In this section we describe briefly the coexisting-phases (CP) method to study the nonhomogeneous phase of nuclear matter with a fixed proton fraction. The basic idea is that matter can be organized into separated regions of higher and lower density, and the geometry of these regions is assumed to be very simple: a lattice of spherical droplets (bubbles), a plane of cylindrical rods (tubes), or an alternating sequence of slabs. The interface between regions is sharp, and it is taken into account by a surface term and a Coulomb one in the energy density. In the spirit of this approach, a single geometry will be the physical one for some given conditions (temperature, density, and proton fraction).

As in [15,16], for a given total density ρ and proton fraction, now defined including the protons present inside the light clusters, the pasta structures are built with different geometrical forms in a background nucleon gas. This is achieved by calculating from the Gibbs conditions the density and the proton fraction of the pasta and of the background gas, so that we have to solve simultaneously the following equations together with Eqs. (19) and (20):

$$P^I = P^{II}, \tag{24}$$

$$\mu_i^I = \mu_i^{II}, \quad i = p, n, t, h, \alpha, d, \tag{25}$$

$$f\rho_c^I + (1 - f)\rho_c^{II} = Y_{pg}\,\rho, \tag{26}$$

where I and II label the higher and the lower density phase, respectively, and f is the volume fraction of phase I,

$$f = \frac{\rho - \rho^{II}}{\rho^I - \rho^{II}}. \tag{27}$$

The total baryonic density ρ is given by Eq. (12), Y_{pg} is the global proton fraction given by

$$Y_{pg} = \frac{\rho_c}{\rho}, \tag{28}$$

and $\rho_c = \rho_p + 2\rho_\alpha + \rho_d + \rho_t + 2\rho_h$ stands for the charge density.

The density of electrons is uniform and taken as $\rho_e = Y_{pg}\,\rho$. The total pressure is given by the sum of the nuclear and electron partial pressures, $P = P_{\rm nucl} + P_e$, where the nuclear contribution $P_{\rm nucl}$ includes the kinetic contribution of each type of particle (nucleons and light clusters) plus the meson contribution. The total energy density of the system is given by

$$\mathcal{E} = f\mathcal{E}^I + (1 - f)\mathcal{E}^{II} + \mathcal{E}_e + \mathcal{E}_{\rm surf} + \mathcal{E}_{\rm Coul}. \tag{29}$$

By minimizing the sum $\mathcal{E}_{\rm surf} + \mathcal{E}_{\rm Coul}$ with respect to the size of the droplet or bubble, rod or tube, or slab one gets [15] $\mathcal{E}_{\rm surf} = 2\mathcal{E}_{\rm Coul}$, and

$$\mathcal{E}_{\rm Coul} = \frac{2F}{4^{2/3}}(e^2\pi\Phi)^{1/3}\left[\sigma D\left(\rho_c^I - \rho_c^{II}\right)\right]^{2/3}, \tag{30}$$

where F is the volume fraction of the inner part ($F = f$ for droplets, rods, and slabs and $F = 1 - f$ for bubbles and tubes), σ is the surface tension, D is the dimension of the system, and Φ is a coefficient depending upon F and D [11,15].

TABLE III. Surface tension parameters fitted within the Thomas-Fermi approximation for NL3, NL3$\omega\rho$, $\mathrm{FSU_{Gold}}$, and IU-FSU parametrizations. The coefficients are for T in MeV and σ_0 is in $\mathrm{MeV/fm^2}$.

	$\tilde{\sigma}(x)$	$a(T)$	$b(T)$	$c(T)$
NL3				
σ_0	1.12307	–	–	–
σ_1	20.7779	–	–	–
a_0	–	0.0121222	0.00792168	–
a_1	− 5.84915	0.01664	-8.2504×10^{-5}	–
a_2	138.839	− 0.00137266	-4.59336×10^{-6}	–
a_3	− 1631.42	4.0257×10^{-5}	-2.81679×10^{-7}	–
a_4	8900.34	–	–	–
a_5	− 21592.3	–	–	–
a_6	20858.6	–	–	–
NL3$\omega\rho$				
σ_0	1.12013	–	–	–
σ_1	14.0774	–	–	–
a_0	–	-5.80451×10^{-5}	0.00725961	− 0.00259094
a_1	− 2.15376	0.0233833	0.000318409	− 0.053756
a_2	57.8455	− 0.00507732	− 0.000104941	0.0114598
a_3	− 431.365	0.000490863	1.19645×10^{-5}	− 0.000354375
a_4	1854.81	-1.59473×10^{-5}	-7.19099×10^{-7}	-4.76451×10^{-5}
a_5	− 3653.96	-7.55062×10^{-8}	1.62087×10^{-8}	2.28389×10^{-6}
a_6	3214.82	–	–	–
$\mathrm{FSU_{Gold}}$				
σ_0	1.1223	–	–	–
σ_1	− 1.45717	–	–	–
a_0	–	− 0.0133789	0.00773356	0.0408077
a_1	− 3.17729	0.0330912	− 0.000240406	− 0.0971609
a_2	− 9.5121	− 0.00786564	4.52523×10^{-5}	0.0195288
a_3	70.5609	0.000902286	-7.64893×10^{-6}	− 0.00140166
a_4	− 155.641	-4.84828×10^{-5}	5.33346×10^{-7}	4.97386×10^{-5}
a_5	154.691	9.56728×10^{-7}	-1.45394×10^{-8}	-1.20803×10^{-6}
a_6	− 58.9476	–	–	–
IU-FSU				
σ_0	1.16473	–	–	–
σ_1	− 0.659167	–	–	–
a_0	–	0.00404325	0.00767923	0.0066774
a_1	− 2.25482	0.00828207	-8.58068×10^{-5}	− 0.0514285
a_2	− 5.64237	− 0.00153301	4.43918×10^{-7}	0.00949505
a_3	37.8471	7.26763×10^{-5}	-5.44453×10^{-7}	− 0.000427613
a_4	− 81.6617	–	–	–
a_5	81.2696	–	–	–
a_6	− 31.0227	–	–	–

Each structure is considered to be in the center of a charge-neutral Wigner-Seitz cell constituted by neutrons, protons, and electrons [2]. The Wigner-Seitz cell is a sphere or cylinder or slab whose volume is the same as the unit bcc cell. In [2] the internal structures are associated with heavy nuclei. Hence, the radius of the droplet (rod or slab), R_D, and of the Wigner-Seitz cell, R_W, are respectively given by

$$R_D = \left[\frac{\sigma D}{4\pi e^2 \left(\rho_c^I - \rho_c^{II}\right)^2 \Phi}\right]^{1/3}, \tag{31}$$

$$R_W = \frac{R_D}{F^{1/D}}. \tag{32}$$

Concerning the surface energy, the authors of [32] have shown how the surface energy affects the appearance of nonspherical pasta structures. Also the authors of [15] state that the appearance of the pasta phase essentially depends on the value of the surface tension. We have fixed the surface tension at different values and confirmed their claim in [16,18], where the surface tension was parametrized in terms of the proton fraction according to the functional proposed in [33], obtained by fitting Thomas-Fermi and Hartree-Fock numerical values with a Skyrme force. In [19] a new prescription was used and the surface energy was fitted to the results obtained from a relativistic Thomas-Fermi calculation and its dependence upon the temperature was taken into account. A mathematical

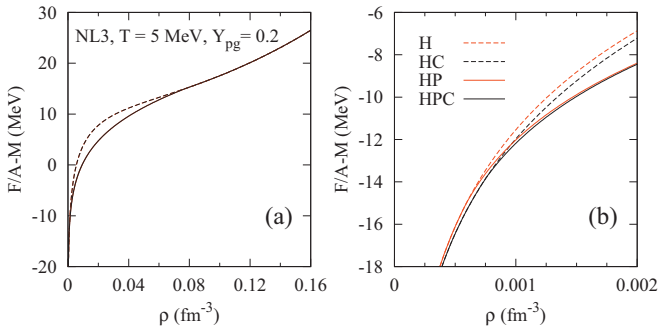

FIG. 2. (Color online) Free energy per particle as a function of the baryonic density for NL3 at $T = 5$ MeV and $Y_{pg} = 0.2$. Four constructions of the equation of state (H, HC, HP, and HPC; see text) are shown: (a) for subsaturation densities and (b) at very low densities. For subsaturation densities, the curves H and HC or HP and HPC are indistinguishable.

formula for σ that gives accurate results for a broad range of neutron excess and for temperatures up to 10 MeV is

$$\sigma(x, T) = \tilde{\sigma}(x)[1 - a(T)xT - b(T)T^2 - c(T)x^2T], \quad (33)$$

where $\tilde{\sigma}(x)$ is the surface tension at $T = 0$ and $x = \delta^2$ stands for the squared relative neutron excess:

$$\delta = \frac{\rho_n - \rho_p}{\rho} = 1 - 2Y_{pg}.$$

In Table III the σ parameters fitted to the Thomas-Fermi approximation results up to $T = 10$ MeV are given. For $T = 10$ MeV the parametrization is good if $Y_{pg} > 0.2$. For lower temperatures, the range of validity extends to lower Y_{pg} values.

IV. RESULTS AND DISCUSSION

In this section we present the results of this work. In Fig. 2 the free energy per particle is shown for four different constructions of the EOS: homogeneous matter (H), homogeneous matter with clusters (HC), mixed homogeneous matter and pasta phase (HP), and finally HP with clusters (HPC). Notice that with HP we mean that both nonhomogeneous matter in five different shapes (droplets, rods, slabs, tubes, and bubbles) and homogeneous matter are computed and the phase with the lowest free energy per particle is the physical one.

The free energy is clearly lowered by the inclusion of both pasta and clusters. However, the pasta phase affects the results in a large density range and leads to a decrease of a few MeV [Fig. 2(a)], whereas the clusters are visible only at very low density and lead to a decrease of $\lesssim$1 MeV [Fig. 2(b)]. Their effect is even smaller in the pasta phase range. It is also seen, as already discussed in [6], that the pasta phase sets in at a larger density when light clusters are included.

The inclusion of the light clusters in the EOS improves the CP method. In fact, the way the surface energy enters in the CP calculation does not allow the appearance of these light nuclei but, as we have seen, their presence is important just below the onset of the pasta phase. We will later verify whether the inclusion of the light clusters explicitly does not correspond to a double description of the small clusters in the pasta phase. In fact, if we include light clusters and obtain droplets formed by four or fewer nucleons the same physical object is being described simultaneously in two distinct ways.

In the more complete case (i.e., HPC), we can see how the fraction of nucleons belonging to different structures changes with the total baryonic density. Nucleons can be free (not clusterized), belong to a light cluster ($A \leqslant 4$), or belong to a heavy one. In our formalism, the role of heavy clusters is played by the high-density part of pasta structures. In the regimes of temperature and proton fraction where a nonhomogeneous phase appears, the following sequence is generally found: homogeneous matter at very low baryonic density, pasta phase at intermediate densities, and then again homogeneous matter at higher densities.

In the nonhomogeneous matter range, the fraction of a generic constituent has contributions from the high-density phase (phase I) and the low-density phase (phase II):

$$Y_i = Y_i^I f \frac{\rho^I}{\rho} + Y_i^{II}(1 - f)\frac{\rho^{II}}{\rho}, \quad (34)$$

where $i = p,\ n,\ \alpha,\ h,\ t,\ d$, and f is the volume fraction of the denser phase defined in (27).

Therefore, we classify the fraction of nucleons as follows:

$$\begin{cases} Y_{p,\text{free}} = Y_p, \\ Y_{n,\text{free}} = Y_n, \\ Y_{\text{light}} = Y_\alpha + Y_h + Y_t + Y_d, \\ Y_{\text{heavy}} = 0 \end{cases} \quad (35)$$

in homogeneous matter at low density,

$$\begin{cases} Y_{p,\text{free}} = Y_p^{II}(1 - f)\frac{\rho^{II}}{\rho}, \\ Y_{n,\text{free}} = Y_n^{II}(1 - f)\frac{\rho^{II}}{\rho}, \\ Y_{\text{light}} = \left(Y_\alpha^{II} + Y_h^{II} + Y_t^{II} + Y_d^{II}\right)(1 - f)\frac{\rho^{II}}{\rho}, \\ Y_{\text{heavy}} = f\frac{\rho^I}{\rho} \end{cases} \quad (36)$$

in the nonhomogeneous phase, and finally

$$\begin{cases} Y_{p,\text{free}} = 0, \\ Y_{n,\text{free}} = 0, \\ Y_{\text{light}} = 0, \\ Y_{\text{heavy}} = 1 \end{cases} \quad (37)$$

in the high-density homogeneous phase.

In Fig. 3 the fractions of nucleons are shown for the NL3 and NL3$\omega\rho$ parametrizations at $T = 5$ MeV and $Y_{pg} = 0.2$. For both parametrizations, matter in the low-density regime is formed by unclusterized neutrons and protons and a light-cluster fraction. The magnitude of this fraction depends on the temperature. At $\rho \sim 0.001$ fm^{-3} the pasta phase sets in. The background low-density gas is constituted mainly by neutrons with a small fraction of protons and light clusters. For densities above 0.08 fm^{-3} there is a transition to dense homogeneous matter, interpreted in the present approach as an infinite cluster.

The differences between the results obtained for NL3 and NL3$\omega\rho$ can be interpreted as a consequence of the effect of the density dependence of the symmetry energy. Both NL3

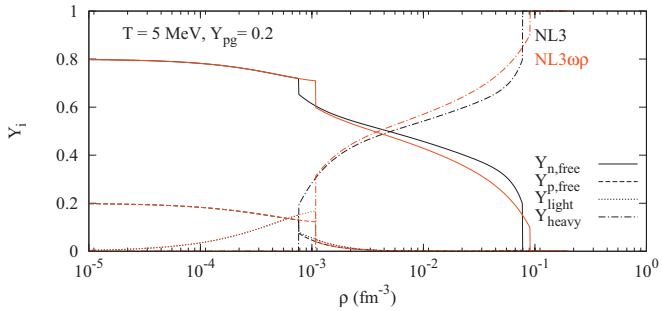

FIG. 3. (Color online) Fractions of nucleons as a function of the density, for the NL3 and NL3$\omega\rho$ parametrizations at $T = 5$ MeV and $Y_{pg} = 0.2$.

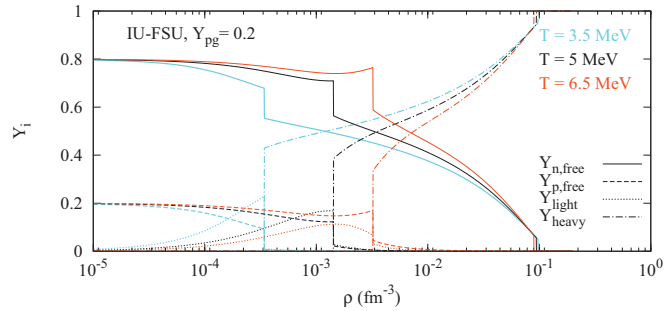

FIG. 5. (Color online) Fractions of nucleons as a function of the density, for the IU-FSU parametrization at $Y_{pg} = 0.2$ and three different temperatures.

and NL3$\omega\rho$ have the same isoscalar properties. However, they differ in the isovector channel; namely, the symmetry energy and its slope at saturation are different, NL3$\omega\rho$ having a smaller symmetry energy and smaller slope at saturation. Below $\rho = 0.1$ fm^{-3} the symmetry energy is larger for NL3$\omega\rho$ while the opposite occurs above that density [see Fig. 1(b)]. It is seen that both models behave in the same way below the onset of the pasta phase: the proton, neutron, and light cluster fractions are practically equal. However, there are noticeable differences in the pasta phase. The most important ones are the onset density of the pasta phase and the fraction of nucleons in the cluster. A smaller symmetry energy slope shifts the onset of the pasta phase of NL3$\omega\rho$ to larger densities because it gives rise to a larger surface energy that hinders the formation of pasta structures. A larger surface energy also gives rise to a smaller fraction of neutrons outside the cluster because it is more difficult for neutrons to drip out. Since neutrons play an important role in the cooling of the crust, the fraction of free neutrons in the pasta phase range will certainly affect the cooling and transport properties of the crust.

We plot in Fig. 4 the fractions of nucleons predicted by the FSU$_{\rm Gold}$ and IU-FSU parametrizations compared to the NL3 results. There are some similarities between these results and those obtained with NL3$\omega\rho$. The onset of the pasta phase density occurs for the IU-FSU parametrization at values slightly higher than in FSU$_{\rm Gold}$ and much higher than in NL3, due to its smaller L and, therefore, larger surface tension. At low densities, the main differences among the three models occur at $\rho \sim 0.001$ fm^{-3} with different proton and light cluster fractions. These differences are mainly due to differences in the density dependence of the isoscalar channel of the EOS. The FSU$_{\rm Gold}$ parametrization has the largest g_s coupling, so, since nucleons have a smaller effective mass, and a larger binding energy per particle, the formation of light clusters is not so favored as in a model where the nucleon effective mass is larger. However, a small fraction of light clusters is still observed in FSU$_{\rm Gold}$, because the onset of the pasta phase occurs at densities larger than in NL3.

The effect of the temperature on the nucleon ratios is examined in Fig. 5, where the results for $T = 3.5$, 5, and 6.5 MeV are shown for the IU-FSU parametrization with $Y_{pg} = 0.2$. The main features of increasing the temperature can be summarized in three points: (a) the onset of the pasta phase (of the core) is shifted to higher (smaller) densities, as already discussed in [34]; (b) the low-density gas of the pasta phase has a larger number of particles; and (c) the light clusters contribution is smaller at densities below the pasta phase onset and larger in the low-density background gas of the pasta phase. These behaviors all occur because when the temperature increases the instability region decreases and there is a larger number of nucleons that drip out of the dense clusters.

The effect of the global proton fraction on the pasta phase is clearly seen in Fig. 6, where the different constituent fractions at densities below 0.1 fm^{-3} are plotted for $Y_{pg} = 0.2$, 0.3, and 0.5 for the IU-FSU parametrization at $T = 5$ MeV. The onset of the pasta phase occurs at larger densities for the more symmetric matter. This is possibly a trend due to the method

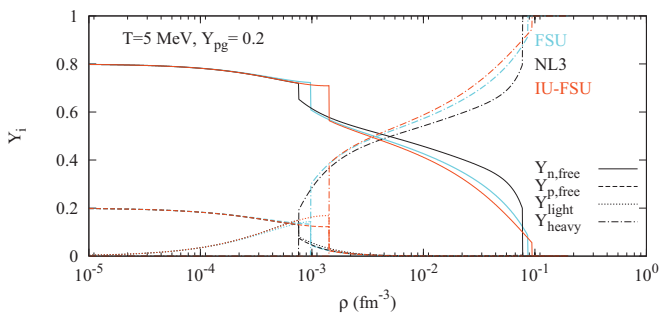

FIG. 4. (Color online) Fractions of nucleons as a function of the density, for the NL3, FSU$_{\rm Gold}$, and IU-FSU parametrizations at $T = 5$ MeV and $Y_{pg} = 0.2$.

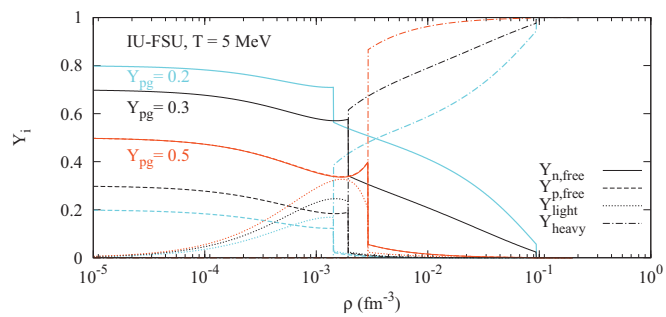

FIG. 6. (Color online) Fractions of nucleons as a function of the density, for the IU-FSU parametrizations at $T = 5$ MeV and several proton fractions.

used for the pasta phase clusters with a zero-thickness surface. In fact, in the pasta calculation within the Thomas-Fermi approach, where the surface is described in a self-consistent way, the opposite occurs [34]. However, if we also consider the light clusters, the onset of the clusterization starts at lower densities for the larger proton fractions. In the pasta phase, the larger proton fractions give rise to clusters with a larger number of nucleons immersed in a gas of nucleons and light clusters with a lower density.

These results allow us to make some comments on the possible consequences of the evolution of a protoneutron star. After the supernova explosion neutrinos are trapped inside the star and we can consider that the lepton fraction is approximately constant, taking a maximum value of 0.4 and decreasing as neutrinos leave the star. A lepton fraction of 0.4 corresponds to a proton fraction of the order of 0.3. During deleptonization the proton fraction of stellar matter decreases and after total deleptonization at densities below 0.08 fm^{-3} the proton fraction is below 0.1. From the behavior obtained in Fig. 6 we conclude that during deleptonization the number of nucleons in the clusters decreases, the low-density background gas of nucleons and light clusters increases, and the onset of the clusterized phase shifts to larger densities.

Next we analyze the properties of the clusters formed in the pasta phase. We consider the droplet geometry because of the finite size of this structure. In particular, we discuss the effects of temperature, isospin asymmetry, and the density dependence of the symmetry energy on the number of nucleons and protons in the droplets, on the onset density of this geometry, and on the transition density to the rod geometry.

We denote by $A_{\rm drop}$ the number of nucleons belonging to a droplet (the type of structure that appears at the lowest densities in the nonhomogeneous phase). We first check whether we are including correctly the light clusters: in fact, we have to check that $A_{\rm drop} > 4$, to confirm that classifying these droplets as heavy clusters is correct. Second, we can compare our results to those obtained in other approaches, [7,8]. We calculate this quantity as

$$A_{\rm drop} = \frac{4\pi}{3} R_D^3 \left[\rho^I - \rho^{II}(Y_p^{II} + Y_n^{II})\right]. \qquad (38)$$

In a similar way, we can compute $Z_{\rm drop}$, the charge content of a droplet. Next we show several figures including our results for both $A_{\rm drop}$ and $Z_{\rm drop}$ for various models, temperatures, and proton fractions.

In Fig. 7 we display the results for different parametrizations: NL3 and NL3$\omega\rho$ in Fig. 7(a) and NL3, FSU$_{\rm Gold}$, and IU-FSU in Fig. 7(b). Here and in the following analogous figures, the solid lines represent $A_{\rm drop}$, and the dashed ones represent $Z_{\rm drop}$. The onset of the droplet phase is characterized by a discontinuity in the number of nucleons inside the cluster: it is necessary a minimum number of nucleons to compensate the surface energy, which is larger for NL3$\omega\rho$. In a Thomas-Fermi calculation, where the surface energy is calculated self-consistently we may expect a less discontinuous behavior. A change in the isovector channel of the model as in NL3$\omega\rho$ leads to a large effect on the number of nucleons, more than doubling this number. As discussed before, a smaller symmetry energy slope corresponds to a larger surface energy and neutrons do not drip out so easily. The number of nucleons obtained within NL3$\omega\rho$ is consistent with the results of [7] within a statistical model, based on the TMA parametrization [35]. We should point out that for NL3 the separation that has been done in light clusters and heavy clusters breaks down for a small proton fraction because, at low densities, the size of the heavy clusters equals the size of the light clusters. The models which include an isoscalar-isovector coupling Λ_v present larger nuclei, the heaviest ones corresponding to IU-FSU. In these models, the appearance of the heavy clusters occurs at similar densities, larger than that obtained for NL3. This again is due to the fact that NL3 has the largest symmetry energy slope at these densities.

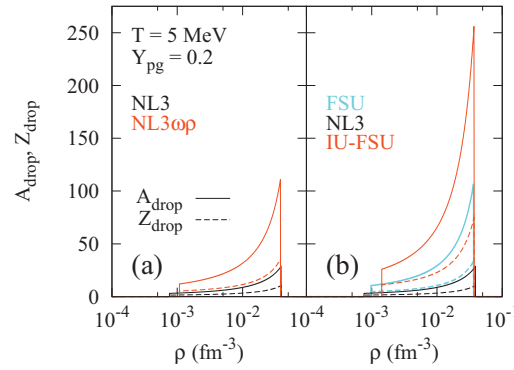

FIG. 7. (Color online) A and Z in a droplet at $T = 5$ MeV and $Y_{pg} = 0.2$: (a) NL3 and NL3$\omega\rho$ parametrizations; (b) NL3, FSU$_{\rm Gold}$, and IU-FSU parametrizations.

In Fig. 8 we plot the radius of the Wigner-Seitz cell together with the droplet radius as a function of density for NL3, NL3$\omega\rho$, FSU$_{\rm Gold}$, and IU-FSU. The ordering of the radii obtained in the different parametrizations reflects perfectly the ordering of their surface tensions [cf. Fig. 1 (b)], which, in turn, is closely linked to the symmetry energy density dependence [cf. Fig. 1(a) and Table II]. NL3 has by far the smallest surface energy at $Y_{pg} = 0.2$, while IU-FSU has the largest [see Fig. 1(b)]: correspondingly, NL3 has the smallest Wigner-Seitz cell and droplets and IU-FSU the largest ones, as shown in Fig. 8.

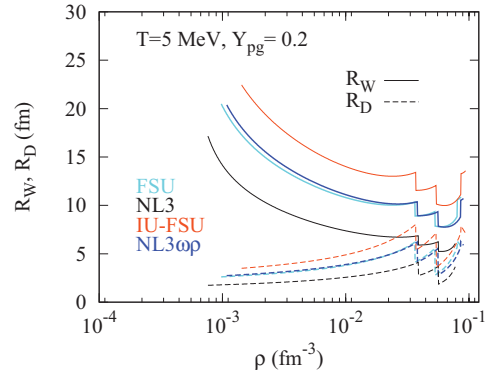

FIG. 8. (Color online) Droplet and Wigner-Seitz cell radius of the clusters for NL3, NL3$\omega\rho$, FSU$_{\rm Gold}$, and IU-FSU calculated at $T = 5$ MeV and $Y_{pg} = 0.2$.

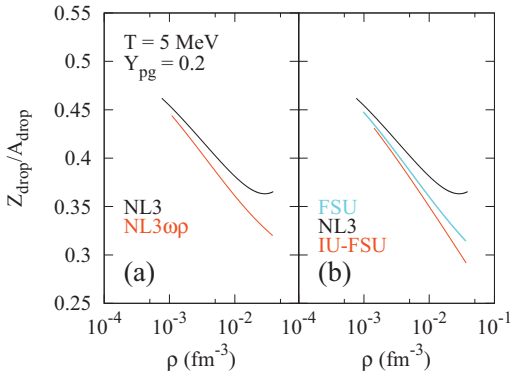

FIG. 9. (Color online) The ratio Z/A in a droplet at $T = 5$ MeV and $Y_{pg} = 0.2$: (a) NL3 and NL3$\omega\rho$ parametrizations; (b) NL3, FSU_{Gold}, and IU-FSU parametrizations.

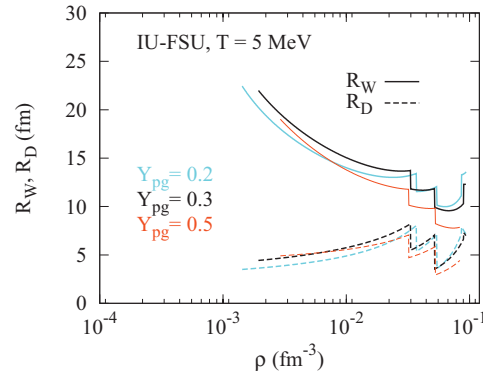

FIG. 11. (Color online) Droplet and Wigner-Seitz cell radii of the clusters for IU-FSU calculated at $T = 5$ MeV and $Y_{pg} = 0.2$, 0.3, and 0.5.

In Fig. 9 the ratio $Z_{\text{drop}}/A_{\text{drop}}$ is plotted as a function of density for the different models we are comparing. We conclude that this ratio decreases with density and is model dependent. A decrease of the proton fraction of the clusters with density was also obtained in [8].

The models with a smaller symmetry energy slope have smaller proton fractions. A smaller slope implies that neutrons drip out of the cluster with more difficulty, giving rise to neutron richer clusters. Also, a smaller slope results in a smaller $\mathcal{E}_{\text{sym}}(\rho)$ above $0.7\rho_0$ [$\simeq 0.1$ fm^{-3}, where approximately all the curves cross; see Fig. 1(a)]. Since the density inside the droplets is between $0.7\rho_0$ and ρ_0, a smaller symmetry energy favors less symmetric clusters.

The dependence of A_{drop} and Z_{drop} on the temperature for $Y_{pg} = 0.2$, and on the proton fraction, for $T = 5$ MeV is plotted in Figs. 10(a) and 10(b), respectively, for the IU-FSU parametrization. Decreasing the temperature increases slightly the number of nucleons in the clusters and strongly decreases the onset density. The transition to the rod geometry seems to be temperature independent.

Isospin asymmetry affects the number of nucleons in the cluster in a nonlinear way, as is seen in Fig. 10(b) for the IU-FSU parametrization. At the onset of the pasta phase the size of the clusters is smaller for the smaller proton fractions. However, there is a faster increase of the cluster size with density when the proton fraction is smaller. In particular, at the transition to the rod geometry we get smaller droplets in symmetric matter. This behavior is also obtained for FSU_{Gold} and NL3$\omega\rho$. However, for NL3, we get a systematic behavior, with smaller proton fractions corresponding to smaller numbers of nucleons in the cluster. In [8], using the Skyrme interaction SKM* with a quite low symmetry energy slope at saturation ($L = 45$ MeV), a cluster size independent of the proton fraction was obtained. On the other hand, the authors of [7] using TMA get at $T = 1$ MeV larger clusters for $Y_{pg} = 0.3$ and smaller ones for $Y_{pg} = 0.5$, and at $T = 5$ MeV larger clusters for $Y_{pg} = 0.3$ and smaller ones for $Y_{pg} = 0.1$. It seems that the proton fraction is not affecting the size of the clusters in a linear way, and this behavior is model dependent. In fact, from Fig. 6 it is seen that the proton fraction with the largest fraction of nucleons in the clusters is $Y_{pg} = 0.5$. However, the number of nucleons in the droplets also depends on their size. In Fig. 11 we show how the size of the Wigner-Seitz cell and droplet radius depend on the density and proton fraction. The number of particles in the droplets is strongly dependent on these two radii.

In Fig. 12 we show for IU-FSU how the proton fraction in the droplets depends on the temperature and on the global proton fraction. Temperature makes droplets richer in protons

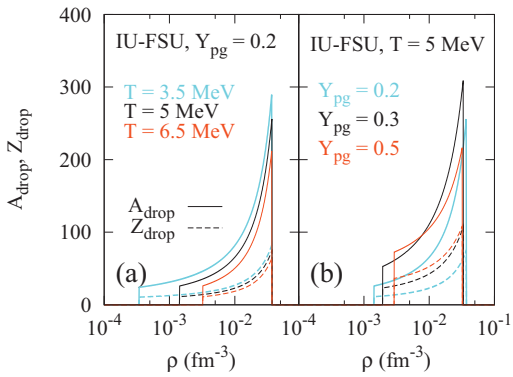

FIG. 10. (Color online) A and Z in a droplet for IU-FSU: (a) $Y_{pg} = 0.2$ and $T = 3.5$, 5, and 6.5 MeV; (b) $T = 5$ MeV and $Y_{pg} = 0.2$, 0.3, and 0.5.

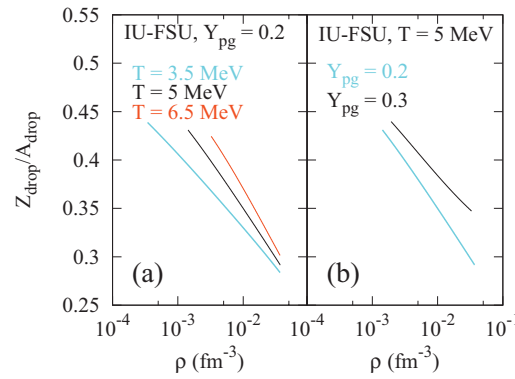

FIG. 12. (Color online) The ratio Z/A in a droplet for IU-FSU: (a) $Y_{pg} = 0.2$ and $T = 3.5$, 5, and 6.5 MeV; (b) $T = 5$ MeV and $Y_{pg} = 0.2$, 0.3, and 0.5.

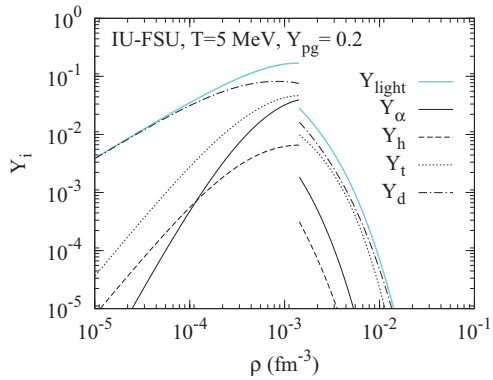

FIG. 13. (Color online) HPC case, showing the various contributions to $Y_{\rm light}$ explicitly for the IU-FSU parametrization at $T = 5$ MeV, $Y_{pg} = 0.2$.

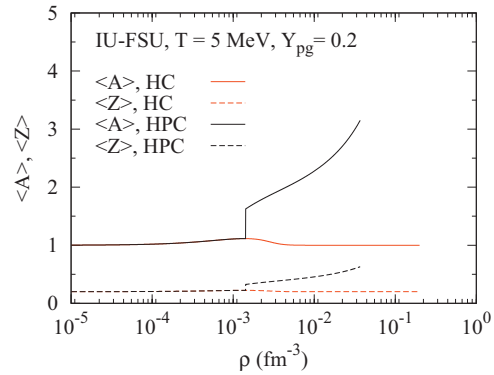

FIG. 14. (Color online) The average size and charge of the constituents present in HC and HPC for the IU-FSU parametrization at $T = 5$ MeV, $Y_{pg} = 0.2$.

and greater isospin asymmetry reduces the proton fraction in the droplets. In fact, temperature helps the evaporation of neutrons from the droplets, increasing the proton fraction in the clusters. On the other hand, increasing the neutron fraction leads naturally to an increase of neutrons in the clusters. These two effects were also obtained in the formalism developed in [8] within a grand-canonical ensemble approach (see left panels of Fig. 25 in Ref. [8]).

To complete the discussion, we now distinguish the contribution of each type of light cluster; i.e., we decompose $Y_{\rm light}$. In Fig. 13 we show the fractions of nucleons belonging to α particles, helions, tritons, and deuterons for IU-FSU at $T = 5$ MeV and $Y_{pg} = 0.2$, as a choice that exemplifies the results we obtain.

Two typical sequences can be identified in the abundances of the various clusters: d, t, h, α at low baryonic density and d, t, α, h at the higher total baryonic density at which clusters are still present. Deviations from this behavior are found for lower temperature ($T = 3.5$ MeV) or higher proton fraction ($Y_{pg} = 0.5$). In general, the dominant contribution comes from the deuterons. At very low density, the sequence reflects the ordering in size: the smaller clusters are more abundant. The difference between t and h, and more precisely the finding that tritons are more abundant than helions, is due to two effects: globally there are more neutrons available and, moreover, the triton is more bound. This last point explains why we find a difference among them also at $Y_{pg} = 0.5$.

For a given temperature, the fraction of α particles at very low density increases with density much faster than the other clusters: this is due to their large binding energy. As a consequence, the fraction of α particles may overcome the fraction of other type of clusters at larger densities. At sufficiently low temperatures, they are the most abundant cluster in HC matter, even for the lowest densities. In HPC matter, their abundance is determined by the density, proton fraction, and temperature of the background gas.

Concerning the dissolution density of each cluster, we find that it increases with increasing temperature; on the other hand, the effect of a larger proton fraction is just to increase slightly the abundance of the clusters (except for tritons); it does not alter their dissolution.

Finally, we show in Fig. 14 the average number of nucleons and the average charge of the constituents in the HC and HPC cases. We consider as constituents the protons, neutrons, α particles, helions, tritons, deuterons, and the droplets. In the low-density limit, the system is composed by free nucleons: in fact, $\langle A\rangle = 1$ and $\langle Z\rangle = 0.2$ in this limit. At intermediate densities, $\langle A\rangle$ increases slightly because of the formation of light clusters. At even higher densities, the behavior is different for the HC and HPC constructions. In the HC case, the clusters dissolve at some density and we get again $\langle A\rangle = 1$, which means a gas of free nucleons. In the HPC case, droplets form, and the average number of nucleons in a cluster increases very rapidly with the density. Concerning the average charge, from the figure it is seen that for the droplets it also increases, but more slowly than $\langle A\rangle$: as already discussed, the isospin asymmetry of the droplets increases with the density.

V. CONCLUSIONS

In the present paper we have investigated the effects caused by the explicit inclusion of four light clusters, namely, α particles, deuterons, tritons, and helions, in homogeneous and nonhomogeneous nuclear matter at low densities. This study is particularly important for understanding the composition of the inner crust of protoneutron stars.

We have chosen to calculate the above-mentioned effects with four different parametrizations of the NLWM because they are characterized by different symmetry energy density dependencies, as seen from the values of their slopes L in Table II.

We have checked that the influence of the light clusters in the free energy per particle is only noticeable at very small densities (up to 0.0025 fm^{-3}) both in homogeneous and pasta phase matter. The inclusion of light clusters lowers the free energy and their effect is smaller in the pasta phase range.

We have analyzed the fractions of nucleons at different temperatures and different proton fractions. The results are model dependent, as expected, and some of the differences are related to the density dependence of the symmetry energy. In the following we identify some of the trends that were found: (a) when temperature increases, the pasta phase appears at

higher densities, an effect already seen without the inclusion of the light clusters; (b) the pasta phase low-density gas, including light clusters, has a larger number of particles at larger temperatures; (c) larger abundances of light clusters occur at densities below the pasta phase onset and their fractions are larger for more symmetric matter; before the onset of the pasta phase their abundances decrease with temperature, and the opposite occurs in the pasta phase; (d) within the coexisting-phases method adopted in the present work, the onset of the pasta phase occurs at lower densities for more asymmetric matter; we believe this is due to the zero-thickness surface approximation and a lack of self-consistency in the calculation of the surface properties. An opposite trend was obtained within a Thomas-Fermi approach [34]. However, if we also consider the light clusters, the onset of clusterization starts at lower densities for the larger proton fractions.

The number of nucleons and the number of charged particles inside the pasta droplets were calculated. It was shown that (a) models with a smaller symmetry energy slope have larger clusters, inside a larger Wigner-Seitz cell, with a larger number of particles and smaller proton fraction; (b) the number of nucleons in the droplets has no linear relation with the global isospin asymmetry of matter and density, showing a strong dependence on the properties of the symmetry energy; (c) the number of nucleons in the clusters decreases if temperature increases; and (d) the fraction of protons in the clusters decreases with density, decreases for more asymmetric matter, and increases when temperature increases.

We have shown that the composition and structure of the pasta phase is quite sensitive to the symmetry energy behavior at low densities. It would be interesting to study the transport properties and neutrino opacity in the pasta phase with light clusters, because these are important quantities in the cooling mechanism of protoneutron stars.

ACKNOWLEDGMENTS

This work was partially supported by the Capes/FCT No. 232/09 bilateral collaboration, CNPq and FAPESC/1373/2010-0 (Brazil), FCT and COMPETE (Portugal) under Projects No. PTDC/FIS/113292/2009 and No. CERN/FP/116366/2010, and Compstar, an ESF Research Networking Programme. S.C. is supported by FCT under Project No. SFRH/BPD/64405/2009.

APPENDIX

The surface tension is obtained by fitting the Thomas-Fermi results with the formula

$$\sigma(x,T) = \tilde{\sigma}(x)[1 - a(T)xT - b(T)T^2 - c(T)x^2T], \quad \text{(A1)}$$

where

$$\begin{aligned}
\tilde{\sigma}(x) &= \sigma_0 \exp(-\sigma_1 x^{3/2})(1 + a_1 x + a_2 x^2 \\
&\quad + a_3 x^3 + a_4 x^4 + a_5 x^5 + a_6 x^6), \\
a(T) &= a_0 + a_1 T + a_2 T^2 + a_3 T^3 + a_4 T^4 + a_5 T^5, \\
b(T) &= a_0 + a_1 T + a_2 T^2 + a_3 T^3 + a_4 T^4 + a_5 T^5, \\
c(T) &= a_0 + a_1 T + a_2 T^2 + a_3 T^3 + a_4 T^4 + a_5 T^5. \quad \text{(A2)}
\end{aligned}$$

Clearly, $\tilde{\sigma}(x)$ is the surface tension at $T = 0$, and σ_0 is its value at $T = 0$ for symmetric matter. Notice moreover that there are a few more terms in these parametrizations as compared to those used in Ref. [19].

[1] J. M. Lattimer and F. D. Swesty, Nucl. Phys. A **535**, 331 (1991).
[2] H. Shen, H. Toki, K. Oyamatsu, and K. Sumiyoshi, Nucl. Phys. A **637**, 435 (1998).
[3] M. Beyer, S. A. Sofianos, C. Kuhrts, G. Roepke, and P. Schuck, Phys. Lett. B **488**, 247 (2000).
[4] C. J. Horowitz and A. Schwenk, Nucl. Phys. A **76**, 55 (2006).
[5] K. Sumiyoshi and G. Röpke, Phys. Rev. C **77**, 055804 (2008).
[6] S. Typel, G. Röpke, T. Klahn, D. Blaschke, and H. H. Wolter, Phys. Rev. C **81**, 015803 (2010).
[7] M. Hempel and J. Schaffner-Bielich, Nucl. Phys. A **837**, 210 (2010).
[8] A. R. Raduta and F. Gulminelli, Phys. Rev. C **82**, 065801 (2010).
[9] G. Röpke, Nucl. Phys. A **867**, 66 (2011).
[10] M. Hempel, J. Schaffner-Bielich, S. Typel, and G. Röpke, Phys. Rev. C **84**, 055804 (2011)
[11] D. G. Ravenhall, C. J. Pethick, and J. R. Wilson, Phys. Rev. Lett. **50**, 2066 (1983).
[12] M. Hashimoto, H. Seki, and M. Yamada, Prog. Theor. Phys. **71**, 320 (1984).
[13] C. J. Horowitz, M. A. Pérez-Garcia, and J. Piekarewicz, Phys. Rev. C **69**, 045804 (2004); C. J. Horowitz, M. A. Perez-Garcia, D. K. Berry, and J. Piekarewicz, *ibid.* **72**, 035801 (2005).
[14] G. Watanabe, K. Sato, K. Yasuoka, and T. Ebisuzaki, Phys. Rev. C **66**, 012801 (2002); **68**, 035806 (2003); **69**, 055805 (2004); H. Sonoda, G. Watanabe, K. Sato, K. Yasuoka, and T. Ebisuzaki, *ibid.* **77**, 035806 (2008).
[15] T. Maruyama, T. Tatsumi, D. N. Voskresensky, T. Tanigawa, and S. Chiba, Phys. Rev. C **72**, 015802 (2005).
[16] S. S. Avancini, D. P. Menezes, M. D. Alloy, J. R. Marinelli, M. M. W. Moraes, and C. Providência, Phys. Rev. C **78**, 015802 (2008).
[17] J. Xu, L. W. Chen, B. A. Li, and H. R. Ma, Phys. Rev. C **79**, 035802 (2009).
[18] S. S. Avancini, L. Brito, J. R. Marinelli, D. P. Menezes, M. M. W. Moraes, C. Providência, and A. M. Santos, Phys. Rev. C **79**, 035804 (2009).
[19] S. S. Avancini, C. C. Barros Jr., D. P. Menezes, and C. Providência, Phys. Rev. C **82**, 025808 (2010).
[20] A. Burrows and J. M. Lattimer, Astrophys. J. **285**, 294 (1984).
[21] M. Ferreira, Master's thesis, University of Coimbra, 2011.
[22] G. A. Lalazissis, J. König, and P. Ring, Phys. Rev. C **55**, 540 (1997).
[23] C. J. Horowitz and J. Piekarewicz, Phys. Rev. Lett. **86**, 5647 (2001); Phys. Rev. C **64**, 062802 (2001); **66**, 055803 (2002).
[24] B. G. Todd-Rutel and J. Piekarewicz, Phys. Rev. Lett. **95**, 122501 (2005).

[25] F. J. Fattoyev, C. J. Horowitz, J. Piekarewicz, and G. Shen, Phys. Rev. C **82**, 055803 (2010).
[26] B. D. Serot and J. D. Walecka, Adv. Nucl. Phys. **16**, 1 (1986).
[27] S. S. Avancini, L. Brito, Ph. Chomaz, D. P. Menezes, and C. Providência, Phys. Rev. C **74**, 024317 (2006).
[28] S. Typel and H. H. Wolter, Nucl. Phys. A **656**, 331 (1999); G. Hua, L. Bo, and M. Di Toro, Phys. Rev. C **62**, 035203 (2000); T. Gaitanos, M. Di Toro, S. Typel, V. Baran, C. Fuchs, V. Greco, and H. H. Wolter, Nucl. Phys. A **732**, 24 (2004).
[29] K. Sumiyoshi, H. Kuwabara, and H. Toki, Nucl. Phys. A **581**, 725 (1995).
[30] H. Mueller and B. D. Serot, Nucl. Phys. A **606**, 508 (1996).
[31] F. J. Fattoyev and J. Piekarewicz, Phys. Rev. C **82**, 025805 (2010).
[32] G. Watanabe, K. Iida, and K. Sato, Nucl. Phys. A **687**, 512 (2001).
[33] J. M. Lattimer, C. J. Pethick, D. G. Ravenhall, and D. Q. Lamb, Nucl. Phys. A **432**, 646 (1985).
[34] S. S. Avancini, S. Chiacchiera, D. P. Menezes, and C. Providência, Phys. Rev. C **82**, 055807 (2010).
[35] H. Toki, D. Hirata, Y. Sugahara, K. Sumiyoshi, and I. Tanihata, Nucl. Phys. A **588**, 357 (1995).